1 Surfaces

We got our first hint of the importance of surface processes in the mass spectrum of a "high vacuum" environment. The spectrum was dominated by water and carbon monoxide, species that represent a small component of the atmosphere, but (in contrast to oxygen, nitrogen and argon) adsorb readily to metal surfaces and desorb at a significant rate at room temperature. Figure 1 shows the idea. Plotted on a log-log plot is the pressure in a model vacuum chamber as a function of time. The initial pump out of the atmospheric gases is over in a matter of a few seconds, followed by a long period in which surface desorption dominates. Where low pressures are important, this stage is typically accelerated by a a "bake out" where the entire vacuum chamber is heated to an elevated temperature (100-400 C) for a period of time ranging from a few hours to a few days to remove adsorbates from the walls. What next limits the pressure is diffusion of atomic hydrogen out of the bulk of the vacuum chamber walls to the surface, where the atoms recombine and desorb as H_2. In rare circumstances, the material can be depleted of hydrogen and the pressure limited only by the actual permeation of gas from outside.

The simplest model for the surface desorption step considers the desorption as a first order process in which the rate is given by

$$\frac{d\sigma}{dt} = \nu \exp^{-E_a/k_bT} \sigma$$

where σ is the particle concentration (in cm^{-2}), k_b is Boltzmann's constant, T the absolute temperature and the kinetic parameters are E_a the activation energy for desorption and ν the imaginatively named preexponential factor. Typical binding energies and the corresponding surface residence times are given in Table 1.

Table 1: Residence time (τ) in seconds for adsorbed molecules

Gas/Surface	Binding Energy (eV)	τ(s) at 77 K	τ(s) at 22 C	τ(s) at 450 C
H_2O/H_2O	0.40	10^{15}	10^{-5}	10^{-9}
H_2O/metal	1.00	-	10^{5}	10^{-5}
H_2/Mo	1.6	-	10^{17}	10^{0}

The surface binding energies are determined by the technique of thermal programmed desorption (TPD) whereby a surface at low temperature is dosed with the species of interest and then the evolution into the gas phase is monitored with the mass spectrometer as the surface temperature is raised in a controlled manner. A particularly rich example of the application of this technique is shown in Fig. 1 for a system involving water and carbon tetrachloride (CCl_4).

1.1 Electronic Spectroscopy

A wide variety of surface analysis involves using electrons as a probe. There is a fundamental reason for this which is illustrated in Fig. 2 which shows the electron mean free path as a function of energy for some different materials. This so called universal curve has a minimum for electron energies of a few hundred eV and the minimum occurs for length of about one lattice spacing. What this means is that if some process generates electrons in this energy range,

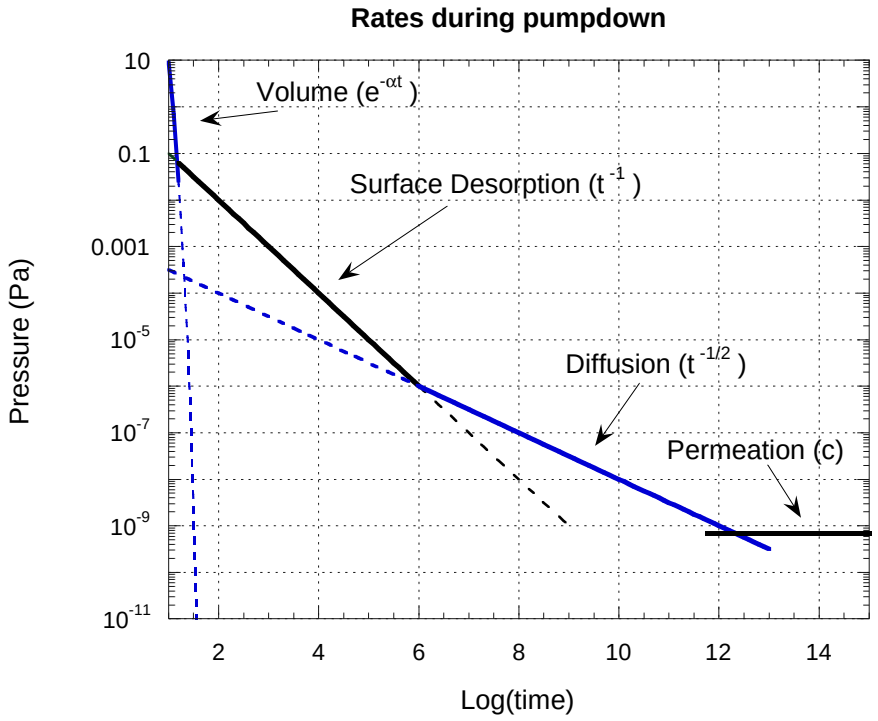

and you have an energy specific electron detector, you can be reasonable sure that you are sensitive to only the surface or near surface layer of the material under study. Electrons originating deeper will scatter inelastically with high probability and not contribute to the energy resolved signal.

Electrons can be generated in and scattered from a surface in a large variety of processes. Figure 1.1 schematically illustrates a few such techniques, each with its own acronym (if your technique does not have an acronym, it hasn't arrived). For any of these techniques to be implemented, a way to analyze the energies of electrons leaving the surface has to be implemented. As with mass spectrometers, this can be done with either a magnetic field, an electric field, a combination of both, or by time-of-flight if the source of the electrons is pulsed. Figure 4 shows several electron spectrometers commonly used in surface science (and in atomic or molecular physics in general).

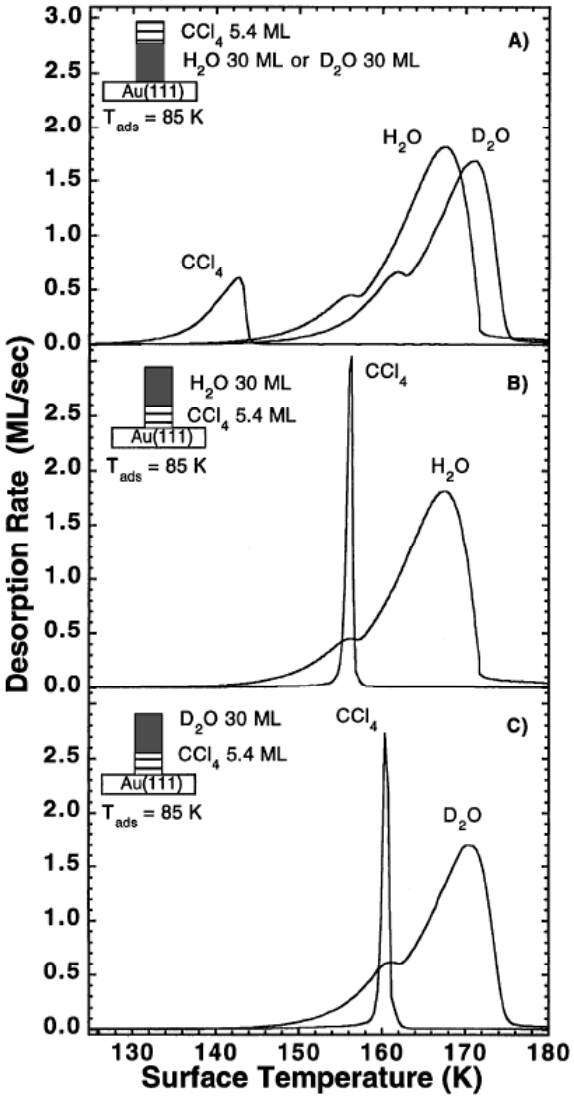

Figure 1: (A) TPD spectra (measured with a quadrupole mass spectrometer) of 5.4 ML CCl_4 grown on top of 30 ML of either H_2O or D_2O ASW. The CCl_4 desorption from either ASW is the same. The bump in the water desorption (156 K for H_2O and 161 K for D_2O) arises from the irreversible phase transformation of ASW into crystalline ice. (B) TPD spectra for 30 ML of ASW (H_2O) grown on top of 5.4 ML of CCl_4. (B) TPD spectra for 30 ML of ASW (D_2O) grown on top of 5.4 ML of CCl_4. The spectra in both (B) and (C) show that the CCl_4 is trapped beneath the ASW dsposit and then desorbs abruptly in concert with the ASW crystallization.

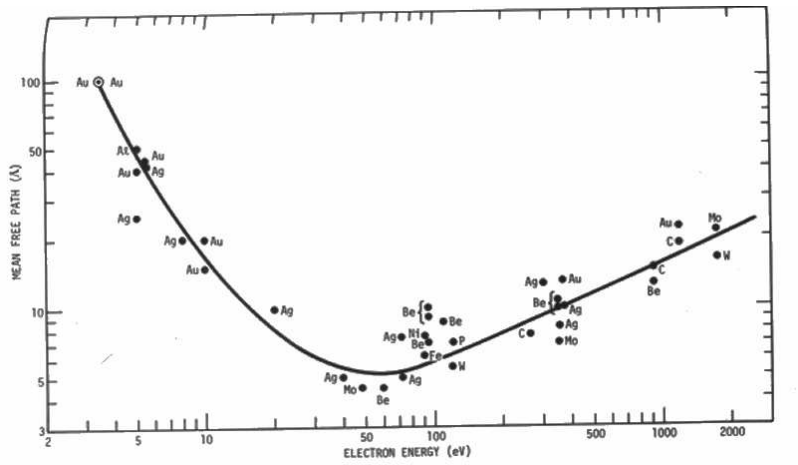

Figure 2: Universal curve for the electron mean free path as a function of electron kinetic energy. Dots indicate individual measurements.

"Chemistry in two dimensions: surfaces," Gabor A. Somorjai, Ithaca, 1981.

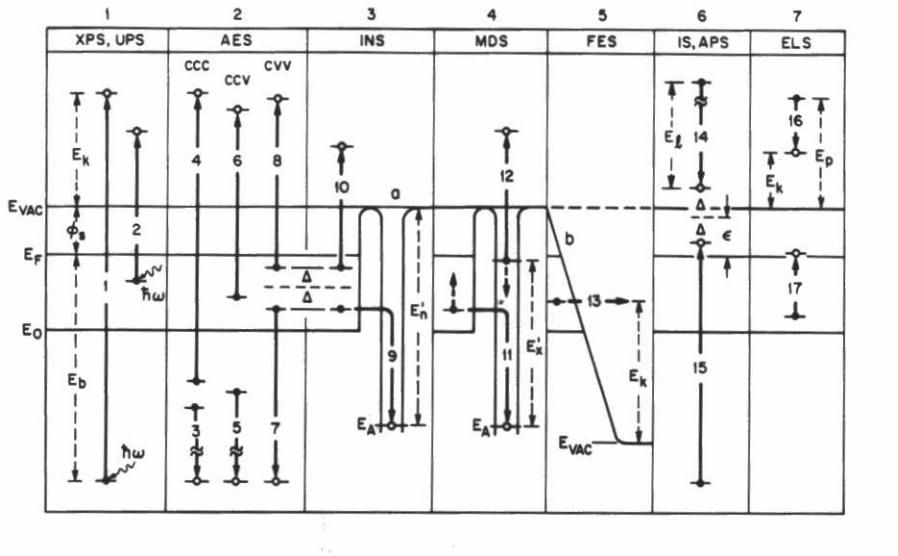

Figure 3: Electronic transitions basic to several electron spectroscopies. E_{vac}, E_F, and E_0 indicate the vacuum level, the Fermi level, and the level of the bottom of the valence band respectively. $\hbar\omega$, E_k, ϕ_s, and E_b are photon energy, electron kinetic energy just outside the surface, surface work function, and electron binding energy, respectively. In panel 2 the three letters involving c (core) and v (valence) designate the types of levels in which the three holes involved in the Auger process lie in order of decreasing binding energy.

"A Physicist's Desk Reference," Second Edition, Herbert L. Anderson, Editor in Chief, American Institute of Physics, 1989.

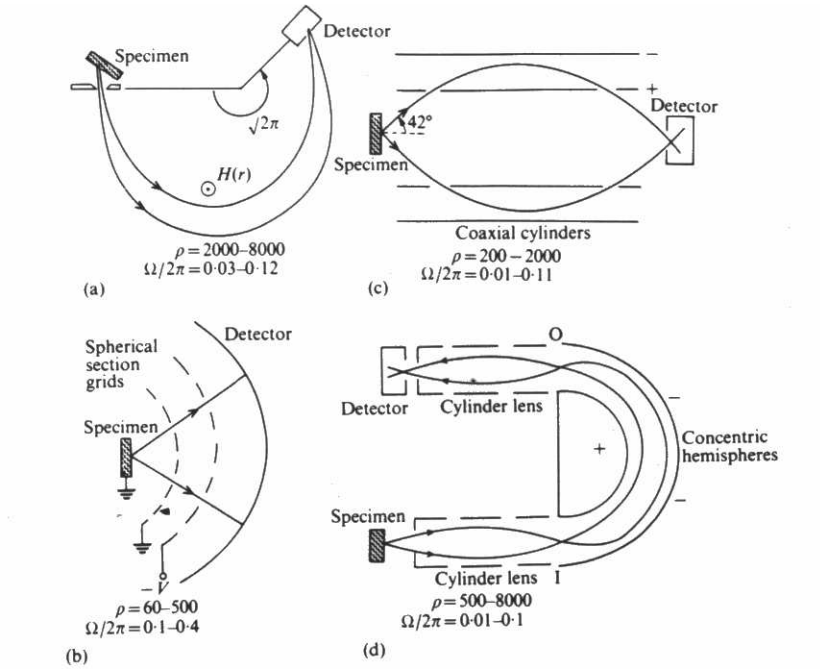

Figure 4: Four methods of electron energy analysis after photoemission of an Auger process. Typically accessible ranges of ρ and $\Omega/2\pi$ are indicated for each method. (a) The magnetic double-focusing spectrometer. Here the field H is made to be proportional to $r^{-1/2}$ for an electron trajectory of radius r. (b) The electrostatic retarding potential analyzer. The potential $-V$ on the second grid results in electron with kinetic energies greater the eV reaching the detector. The grids and detector are concentric spherical sections with their centers on the sampling surface and at the center of the region of electron emission. (c) The electrostatic cylindrical mirror analyszer (CMA). Appropriate potentials on the outer and inner cylinders result in electrons with a particular kinetic energy being focused at the detector aperture. (d) The electrostatic concentric hemispherical analyzer (CHA). The electron source on the sample surface is focused on the entrance aperture I of the analyzer. With appropriate potentials on the inner and outer hemispheres electrons with a particular kinetic energy are focused on the output aperture O. The three-element output lens then focuses this image on to the (real) aperture of the detector.

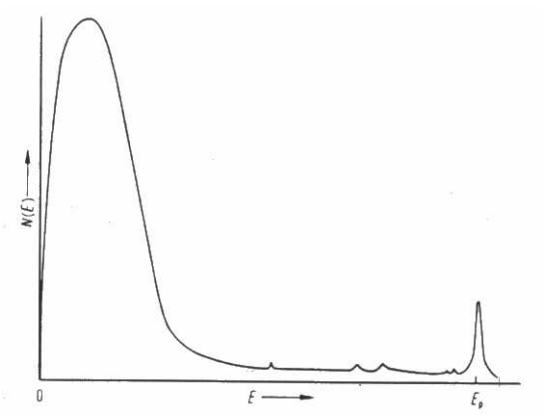

Figure 5: Experimental number of scattered electrons N(E) of energy E versus electron energy E.

"Chemistry in two dimensions: surfaces," Gabor A. Somorjai, Ithaca, 1981.

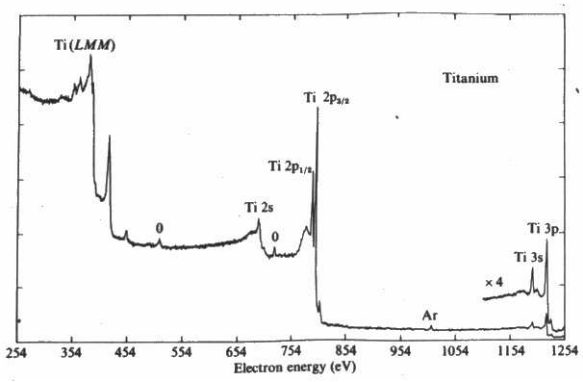

Figure 6: XPS electron energy spectrum from a titanium target illuminated with Mg Kα radiation.

"Physics at Surfaces," Andrew Zangwill, Cambridge University Press, 1988, Chapters 2 and 3.

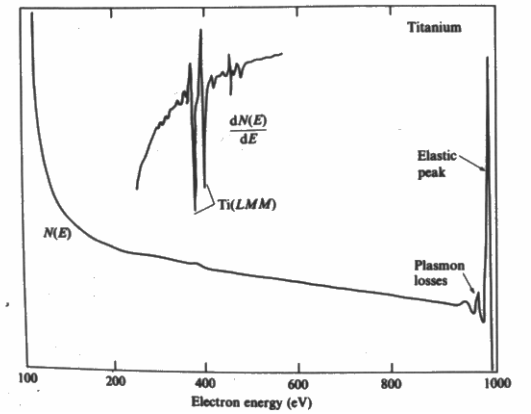

Figure 7: N(E) and dN(E)/dE for electrons backscattered from a titanium target after bombardment with 1 keV electrons.

"Physics at Surfaces," Andrew Zangwill, Cambridge University Press, 1988, Chapters 2 and 3.

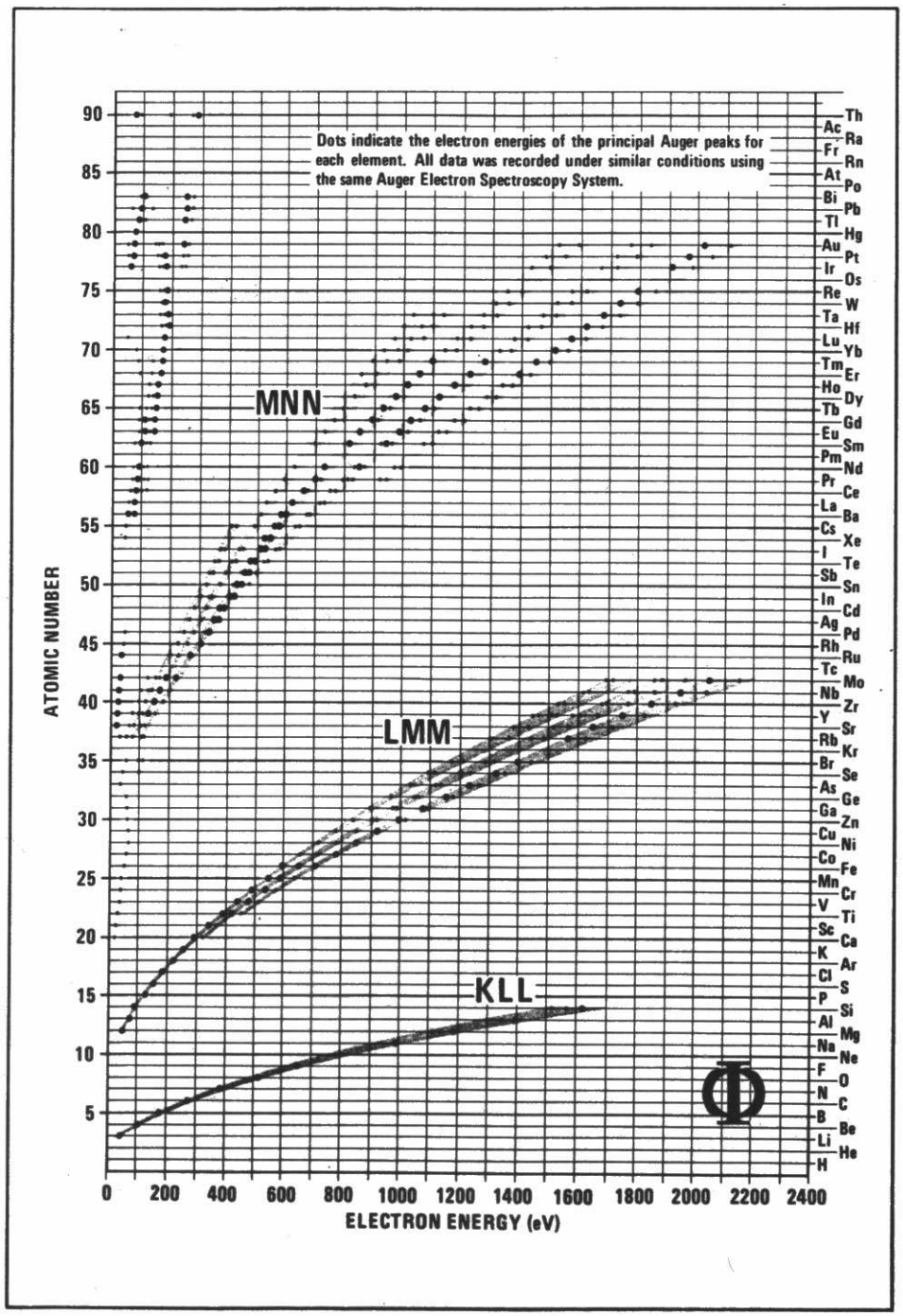

3. Chart of Principal Auger Electron Energies

Figure 8: Chart of Auger electron transitions and energies.

"Handbook of Auger Electron Spectroscopy," Palmberg, Riach, Wber and MacDonald, Physical Electronics Industries, 1972.

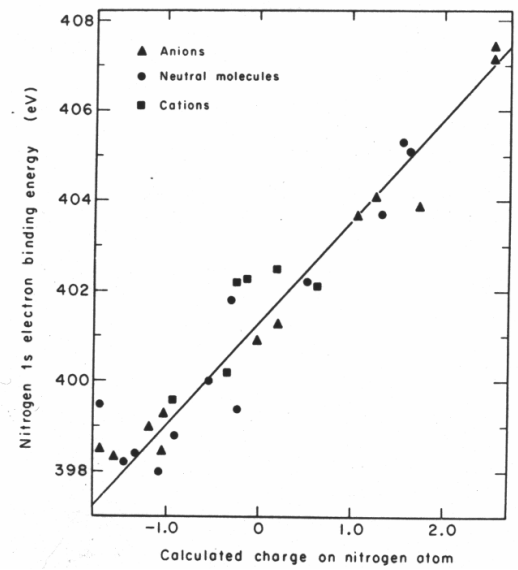

Figure 9: 1s electronic binding energy shifts in nitrogen, indicating the different photoelectron energies observed in various chemical environments.

"Chemistry in two dimensions: surfaces," Gabor A. Somorjai, Ithaca, 1981.

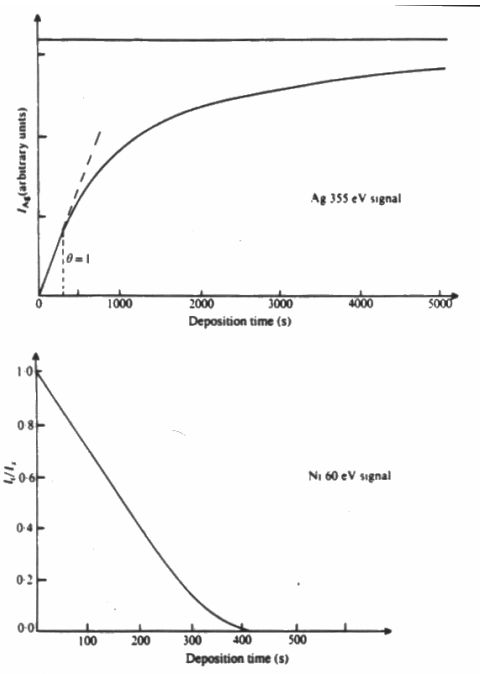

Figure 10: The growth of a silver MNN Auger signal at 355 eV and decay of a nickel MVV Auger signal at 60 eV as silver is deposited at constant rate upon Ni(100). The silver grows up monolayer by monolayer. The break point in the rising curve for silver occurs at a coverage of on monolayer, because at greater coverages the outermost silver atoms shield the first monolayer.

"Chemistry in two dimensions: surfaces," Gabor A. Somorjai, Ithaca, 1981.

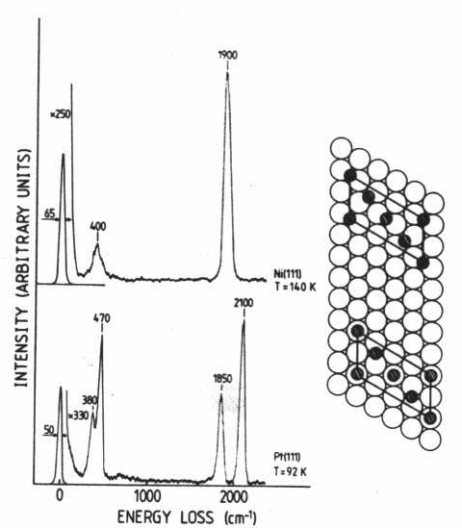

Figure 11: Electron energy loss spectra of the Ni(111) and Pt(111) surfaces, each covered with half a monolayer of CO which orders into a c(4x2) overlayer. On the nickel surface the vibration spectrum indicates only a single CO species in a site of high symmetry. The only possibility for positioning the two-dimensional CO lattice on the surface consistent with the single type of adsorption site is to place all CO molecules into twofold bridges. By similar reasoning, half the CO molecules must occupy on-top sites on the Pt(111) surface. This example shows how powerful the *in situ* comparison of vibrational spectra and diffraction pattern can be, since a qualitative structure analysis is achieved without analyzing diffraction intensities.

"Electron Energy Loss Spectroscopy and Surface Vibrations," H. Ibach and D. L. Mills, Academic Press, 1982.

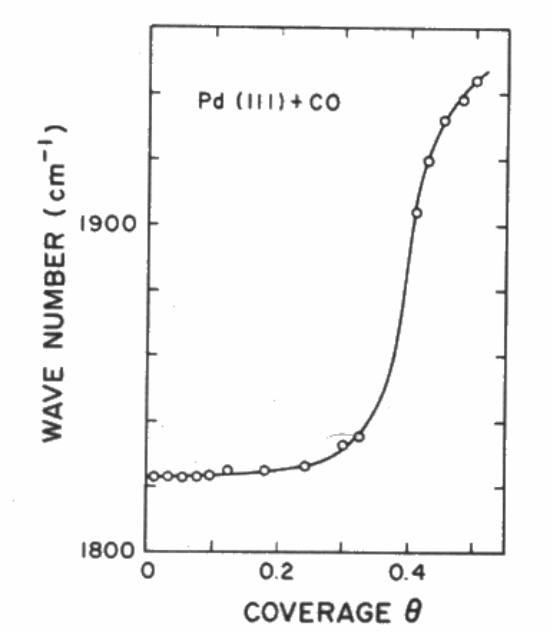

Figure 12: CO stretching frequency versus coverage for Pd(111) at room temperature. The jump in the frequency by $\tilde{6}0$ cm^{-1} is caused by the change of the adsorption site from a threefold bridge to a twofold bridge. The coverage scale was calibrated at $\theta = 0.33$. The scale need not be linear for high coverages since the coverages apparently were calculated from the infrared intensities.

"Electron Energy Loss Spectroscopy and Surface Vibrations," H. Ibach and D. L. Mills, Academic Press, 1982.